Available online at www.sciencedirect.com
SCIENCE DIRECT
Journal of Catalysis 230 (2005) 98–108
JOURNAL OF CATALYSIS
www.elsevier.com/locate/jcat

# In situ, Cr *K*-edge XAS study on the Phillips catalyst: activation and ethylene polymerization

E. Groppo [a], C. Prestipino [a,*], F. Cesano [a], F. Bonino [a], S. Bordiga [a], C. Lamberti [a,*], P.C. Thüne [b], J.W. Niemantsverdriet [b], A. Zecchina [a]

[a] *Department of Inorganic, Physical and Materials Chemistry, and NIS (Centre of Excellence), University of Torino, Via P. Giuria 7, I-10125 Torino, Italy*
[b] *Schuit Institute of Catalysis, Eindhoven University of Technology, 5600 MB Eindhoven, The Netherlands*

Received 27 July 2004; revised 11 November 2004; accepted 12 November 2004

Available online 28 December 2004

**Abstract**

In this in situ EXAFS and XANES study on the Phillips ethylene-polymerization $Cr/SiO_2$ catalyst, two polymerization routes are investigated and compared. The first mimics that adopted in industrial plants, where ethylene is dosed directly on the oxidized catalyst, while in the second the oxidized catalyst is first reduced by CO at 623 K. On this reduced catalyst $C_2H_4$ polymerization has been investigated at room temperature and at 373 K. To allow experiments in transmission mode, a Cr loading of 4 wt% has been adopted. At this loading a fraction of clustered $Cr_2O_3$ particles has been observed and quantified. The use of a third-generation synchrotron radiation source has allowed us to improve the energy resolution and signal-to-noise ratio of the XANES data, allowing us to determine the fraction of Cr sites involved in the polymerization reaction. This number represents an upper limit of the active sites. Preliminary ReflEXAFS experiments have been performed on a model catalyst prepared by impregnation of Cr on a flat Si(100) substrate covered by a thin layer of amorphous silica. Experiments have been performed ex situ on the grafted catalyst (i.e., after impregnation and thermal activation) and at the end of the polymerization stage.


## 1. Introduction

The $Cr/SiO_2$ Phillips catalyst, patented in 1958 by Hogan and Banks [1], is currently responsible for the commercial production of more than one-third of all of the polyethylene sold worldwide [2,3]. Notwithstanding its industrial importance and the numerous efforts made to elucidate the structure of its active sites and the polymerization mechanism, its chemistry remains controversial; the same holds for the estimation of the number of really active sites [4,5]. The Phillips catalyst is obtained by reaction of the hydroxyl groups present on the silica surface with chromic acid. A typical catalyst contains about 0.5–1.0 wt% Cr, corresponding to about 0.2–0.4 Cr atoms/$nm^2$, for a standard silica with a surface area of 400 $m^2\,g^{-1}$. The polymerization activity increases with the chromium loading up to a maximum corresponding to a Cr loading of about 1.0 wt%, as demonstrated by the recent work of van Kimmenade et al. [6]. This suggests that, for higher loadings, the activity of the additional Cr species is negligible.

The anchorage reaction has been demonstrated over the years by means of several techniques, such as infrared spectroscopy [7–9], UV–Vis diffuse reflectance spectroscopy [10], mass spectrometry [4] (with $CrO_2Cl_2$ and silica, which show the release of HCl), and differential thermal analysis [11]. Conversely, the molecular structure of the anchored Cr(VI) is still a strong point of discussion in the literature, and several molecular structures (monochromate, dichromate, polychromate, etc.) have been proposed [3–5,10,12,13]. The reason for this probably lies in the complex redox and coordination chemistry of chromium, in combination with the heterogeneity of the silica surface. The nature of the silica support (e.g., specific surface area, porosity, concentration of surface hydroxyls), the chromium loading,

* Corresponding authors. Fax: +390 11 6707855.
*E-mail addresses:* carmelo.prestipino@unito.it (C. Prestipino), carlo.lamberti@unito.it (C. Lamberti).

0021-9517/$ – see front matter 
doi:10.1016/j.jcat.2004.11.017

and the activation method (e.g., maximum temperature, heating rate, total calcination time, and calcination atmosphere) play a synergic role in the determination of the distribution of chemical states of the supported chromium [5].

In industrial plants, polyethylene is produced by feeding of the Phillips catalyst with ethylene at 373–423 K; an induction time is observed prior to the onset of the polymerization. This is attributed to a reduction phase, during which Cr(VI) is reduced to Cr(II) by ethylene [4]. To discriminate between the reduction and the polymerization phases, a simplified version of the catalyst has been obtained by reduction of the surface chromate precursors with CO at 623 K [4,5,7,14]. In the following, the CO-reduced catalyst is referred to as the "model" catalyst, to distinguish it from the "ethylene-reduced" catalyst. According to literature data, no significant difference in the polymerization products has been found between model and ethylene-reduced catalysts [4,15]. Another way to simplify the problem has been suggested more recently by Thüne et al. [6,16,17], who prepared a model catalyst by impregnating Cr on a flat Si(100) substrate covered by a thin layer of amorphous silica [hereafter called $CrO_x/SiO_2/Si(100)$]. In this way, one can apply the typical surface science methods (XPS, AFM, SIMS, RBS, etc.) to this system and obtain a smaller degree of heterogeneity of Cr species; that is, these catalysts feature exclusively surface monochromate species (no $Cr_2O_3$ clusters) after thermal activation (calcinations in dry air) above 725 K.

The structure of Cr(II) and, to a lesser extent, the average valence state of the reduced chromium on the silica surface have been widely investigated in the past with several spectroscopic and chemical techniques. Using XPS, UV–Vis, and IR spectroscopies, several authors [3,5,7,12,13,18–27] found that the average oxidation state of Cr in the model catalyst is just above 2; here the catalyst comprises mainly anchored Cr(II) and a variable amount of pseudo-octahedral Cr(III) species (presumably in the form of $\alpha$-$Cr_2O_3$).

From this brief introduction, it is clear that the problem of the structure of chromium on the Phillips catalyst is still an open question. As its understanding is of fundamental importance in the determination of the polymerization mechanisms, continuous efforts are being devoted to finding a unifying picture. For this task XAS is a powerful technique for understanding local geometry and electronic structures and could in principle be very useful in understanding the local structure and the oxidation state of chromium species [28–31]. Moreover, the atomic selectivity of XAS spectroscopies is particularly important when one is dealing with diluted systems. Nevertheless, in contrast to the large number of XANES studies on various chromium compounds reported in the past [32,33], only a few XAS works appeared on the Phillips catalyst or on related systems [10,34,35]. Two main reasons could be tentatively proposed to account for this lack. On the experimental side, the high reactivity of the reduced catalysts toward $O_2$ and $H_2O$ requires an extremely severe control of the atmosphere, which is not easily transferred from the laboratory to a synchrotron beamline. With respect to data interpretation, the possible co-presence of different local environments of the chromium species makes the data analysis complex and delicate.

The aim of this work is to follow by XAS the local structure and the oxidation state of Cr sites in the Phillips catalyst during the activation procedure and, for the first time, during interaction with ethylene. In particular, we are interested in singling out the possible difference between the model system and the ethylene-reduced system. From this study, it emerges that the XAS data of a 4 wt% loaded Phillips catalyst cannot be correctly explained without taking into consideration an important fraction of $Cr_2O_3$ nanoparticles. This observation is particularly important for avoiding a misleading interpretation of both past and future XAS results for analogous $Cr/SiO_2$ systems. Furthermore, we demonstrate that it is possible to correlate the fraction of Cr sites involved in the polymerization by means of a XANES technique, by following the erosion of the Cr(II) fingerprint at 5996 eV and the increase in the intensity of the white line.

## 2. Experimental and methods

### 2.1. Experimental

The $Cr/SiO_2$ catalyst was obtained by a procedure described elsewhere [4,5,25,27,36,37], with a Cr loading of 4 wt% on a 400 $m^2/g$ silica support, which is equivalent to a nominal chromium density of 1.2 $Cr/nm^2$. This loading has been chosen to obtain the lowest Cr content that gives an acceptable signal-to-noise ratio in a transmission XAS measurement [10]. Lower Cr loadings require the use of fluorescence geometry [34]. For XAS measurements the catalyst powder was pressed into a thin pellet and transferred to an X-ray cell designed to allow thermal treatments of the sample either under high vacuum or in the presence of gases [38]. After the activation and oxidation steps at 773 K, two different procedures were followed: (i) a reduction step at 623 K followed by CO removal at the same temperature, thus obtaining the so-called model catalyst; (ii) a reduction step in $C_2H_4$ at 523 K followed by evacuation at the same temperature, thus obtaining the so-called ethylene-reduced catalyst.

Transmission XANES spectra were collected at the ESRF (GILDA BM8). The monochromator was equipped with two Si(111) crystals, and harmonic rejection was achieved with mirrors. To ensure very high-quality XANES spectra, sampled in the edge region every 0.2 eV (with an integration time of 5 s/point), the geometry of the beamline was optimized to improve the energy resolution: vertical slits, located 23 m from the source, were set to 0.4 mm, ensuring an actual energy resolution better than 0.3 eV at 6 keV. The following experimental geometry was adopted: (1) $I_0$ counter (ionization detector filled with 1 bar $N_2$, with an efficiency of 10%); (2) sample; (3) $I_1$ counter (ionization detector filled with 100 mbar Ar, with an efficiency of 80%); (4) chromium

metal foil; (5) $I_2$ counter (photodetector). This setup allows a direct energy/angle calibration for each spectrum, avoiding any problem related to small energy shifts as already proved in previous high-resolution XANES studies [39–43]. The first maximum of the XANES derivative spectrum of the Cr metal foil has been defined as 5989.0 eV.

EXAFS data were acquired up to 6800 eV with a variable sampling step in energy, giving rise to $\Delta k_{\max} = 0.05$ Å$^{-1}$, and an integration time of 5 s/point. Three spectra were acquired for each condition and averaged before data analysis, which was performed with Klementev's programs [44,45]. We collected preliminary ex situ XANES spectra in ReflEXAFS mode, using a single-element germanium detector to collect the Cr fluorescence, in the ReflEXAFS chamber of the GILDA BM8 beamline at the ESRF [46] on a $CrO_x/SiO_2/Si(100)$ model catalyst (incidence angle 4 mrad). The sampling steps are the same as adopted for the transmission experiments, and an integration time of 40 s/points was used. The samples were prepared at the Schuit Institute of Catalysis (Eindhoven University of Technology, the Netherlands) as described elsewhere [16], with a Cr loading of 4 Cr atoms/100 Å$^2$. Ex situ experiments were performed on the grafted catalyst (i.e., after impregnation and thermal activation) and at the end of the polymerization stage.

The diffuse reflectance UV–Vis spectra were obtained with a Perkin Elmer Lambda 19 spectrophotometer equipped with a reflectance sphere. The XRD pattern has been corrected with Huber G670 instrument working in the Guinier geometry and equipped with a Cu-$K_{\alpha 1}$ anode.

### 2.2. Methods

In this section a few words will be devoted to the methodology adopted to extract quantitative information from the EXAFS data when more than a phase is present. The procedure is a simplified version of that described in Ref. [47]. A conventional EXAFS analysis is usually performed on samples with a single chemical species, that is, all of the absorbing atoms have the same local coordination. In this case the value obtained by EXAFS analysis is an evaluation of the real structural parameters around the absorber atom. If more than a single chemical species is present in the sample, the EXAFS signal is the sum of the signals corresponding to all phases. In such a case the fit must be performed with the use of a number of theoretical contributions equal to the number of chemical species present in the sample. This means that, in the simple case of a system composed of only two phases, the fitting model will include two different contributions, where in principle the coordination number ($N$), the distance ($R$), the Debye–Waller factor (DW), and the energy shift ($\Delta E$) should be optimized, resulting in eight fitting parameters. The coordination numbers obtained by the fit are proportional to the real ones according to the following relationships:

$$N_{\text{fit}}(\text{phase 1}) = N(\text{phase 1})x,$$

$$N_{\text{fit}}(\text{phase 2}) = N(\text{phase 2})(1-x),$$

where $N$ and $N_{\text{fit}}$ are the real coordination numbers and that obtained by the best fit procedure (in both phases 1 and 2), respectively, and $x$ is the atomic fraction of the absorber in the first phase. Conversely, the distances and the DW factors obtained by the best fit are the correct evaluation of these parameters for both of the phases present in the sample.

Note that this procedure has already been successfully adopted in the following cases: (i) co-presence of surface copper aluminate, $CuCl_2$, and paratacamite in catalysts for the ethylene oxychlorination reaction [47]; (ii) co-presence of three different Cu sites in copper-exchanged Y zeolite [48]; (iii) co-presence of three different Ag sites in silver-exchanged Y zeolite [49]. In the last two cases, the local environment and the relative population of different cationic sites were previously determined by Rietveld refinement of high-resolution XRPD data collected with a synchrotron radiation source (BM16 at the ESRF). The high quality of the EXAFS fits obtained by the optimization of only Debye–Waller factors and $\Delta E$ parameters (the coordination numbers and the distances fixed by XRPD analysis) represents a good test of the validity of this multiphase approach to EXAFS data analysis.

## 3. Results and discussion

### 3.1. Previous UV–Vis and XRD characterization

As a Cr loading of 4 wt% corresponds to about 4 to 8 times the normal Cr loading used in industrial application [5], a pre-screening of the Cr species present on the sample is mandatory. This study was performed with UV–Vis DRS spectroscopy; the results are reported in Fig. 1 [before and after reduction, parts (a) and (b), respectively (black full lines)]. As a model for dispersed Cr(VI) or Cr(II) species [parts (a) and (b), respectively], a similar catalyst prepared with a Cr loading of 0.5 wt% (and subjected to the same treatments) was used (full gray lines). $\alpha$-$Cr_2O_3$ is used as a model of aggregated Cr(III) oxide (dashed lines) in both parts.

The isolated Cr(VI) species on the oxidized sample (Fig. 1a, full gray line) gives rise to two main components at about 30,000 and 21,500 cm$^{-1}$, ascribed in the literature [13,18,50] to oxygen-to-chromium charge-transfer (CT) transitions. The UV–Vis spectrum of $\alpha$-$Cr_2O_3$ (dashed line in Figs. 1a or b) is characterized by an oxygen-to-chromium CT again around 30,000 cm$^{-1}$ and by two $d$–$d$ transitions at 21,500 and 16,500 cm$^{-1}$ [51]. Although components around 30,000 and 21,500 cm$^{-1}$ are present on both isolated Cr(VI) and clustered Cr(III) in octahedral symmetry, the presence of the component at 16,500 cm$^{-1}$ in the spectrum of the 4 wt% sample confirms that a fraction of $Cr_2O_3$ particles is present

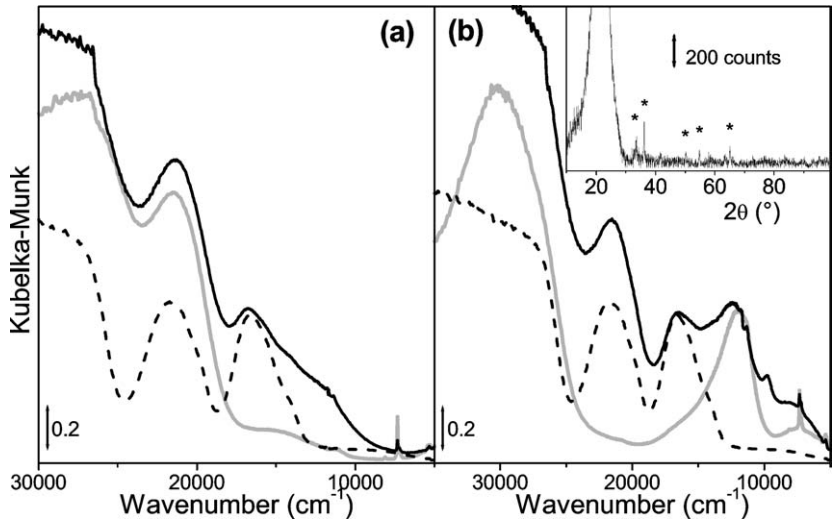


Fig. 1. UV–Vis spectra of $Cr/SiO_2$ at a Cr loading of 0.5 and 4.0 wt% (gray and black full lines, respectively) (a) before and (b) after reduction in CO. For comparison, in both parts the spectrum of $\alpha$-$Cr_2O_3$ (dashed line) is also reported. The inset of part (b) reports the XRD pattern of the reduced catalyst (4.0 wt%) collected with a Cu anode. Labeled with an $*$ are the reflections ascribable to the $\alpha$-$Cr_2O_3$ phase.

at such Cr loadings. This is further demonstrated by the UV–Vis spectrum obtained after CO reduction (Fig. 1b, full black line). Together with the two *d–d* transitions at 12,000 and 7500 $cm^{-1}$, the only peaks present in the 0.5 wt% sample and due to Cr(II) species in a distorted tetrahedral environment [5], clear absorptions at 21,500 and 16,500 $cm^{-1}$, are evident in the full black line in Fig. 1b.

The DRS UV–Vis results are further confirmed by XRD analysis. The reported XRD pattern, shown for the reduced catalyst in the inset of Fig. 1b, is dominated by the huge and broad scattering of the amorphous support in the 10–30° $2\theta$ range. A minor trace of $\alpha$-$Cr_2O_3$ particles sufficiently large to be detected by XRD is evident (see peaks labeled with $*$ in the inset of Fig. 1b). The importance of the bands at 21,500 and 16,500 $cm^{-1}$ in the UV–Vis spectrum, compared with the relative weakness of the reflections of the $\alpha$-$Cr_2O_3$ phase, suggests that most of the $Cr_2O_3$ phase could be composed of particles sufficiently small to escape XRD detection. As two Cr phases are unavoidably present in a 4 wt% sample, particular approaches are required in the EXAFS data analysis, (see Section 2.2). The EXAFS data analysis is discussed in detail in Section 3.2.2.

### *3.2. Activation of the model catalyst and comparison with reference compounds*

#### *3.2.1. XANES data*

Fig. 2 shows high-resolution XANES spectra for the $Cr/SiO_2$ catalyst after oxidation at 773 K (dotted black curve) together with that for the catalyst after reduction in CO at 623 K (black curve). For comparison, the XANES spectra for $CrO_3$ (dotted gray curve) and $\alpha$-$Cr_2O_3$ (gray curve), in which Cr species have a well-defined geometry and oxidation state (+6 and +3, respectively), are also reported. Quantitative values extracted from the spectra reported in Fig. 2 have been summarized in Tables 1–3.

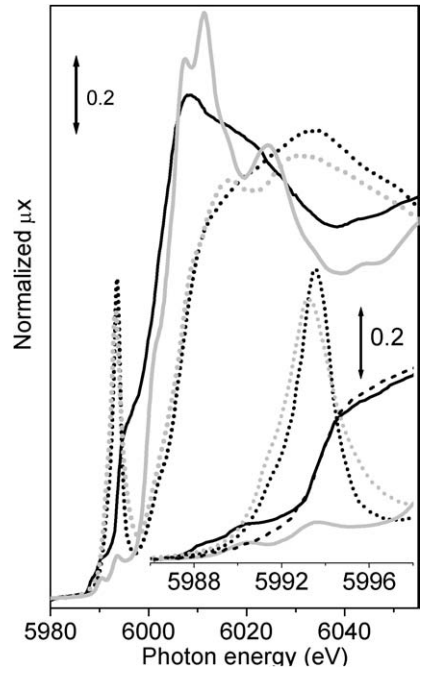


Fig. 2. High resolution XANES spectra of the $Cr/SiO_2$ Phillips catalyst after oxidation at 773 K (black dotted line) and subsequent reduction in CO at 623 K (black line). For comparison also the spectra of $CrO_3$ (dotted gray line) and of $\alpha$-$Cr_2O_3$ (gray line) model compounds are reported. The inset reports a magnification of the pre-edge features; here also the spectrum of the $[Cr(OCOCH_3)_2 \cdot H_2O]_2$ model compound is reported (dashed line).

Starting with the oxidized samples, it is evident that the edge of the oxidized catalyst coincides (within 0.3 eV) with that of $CrO_3$, confirming that Cr species are anchored as Cr(VI) on the silica surface. This agrees well with the literature data based on different spectroscopic laboratory techniques (UV–Vis, Raman, XPS) [9,13,16,17,19,20] and with the previous XANES work of Weckhuysen et al. [10]. A second evident feature is the pre-edge peak at 5993.5 eV typi-

Table 1
XANES features of oxidized Cr(VI) species in $T_d$ symmetry

| Sample | Pre-edge | | | Edge | | | |
|---|---|---|---|---|---|---|---|
| | Position (eV) | Intensity (norm. abs.) | FWHM (eV) | Feature 1 | | Feature 2 | |
| | | | | Position (eV) | Intensity (norm. abs.) | Position (eV) | Intensity (norm. abs.) |
| $CrO_3$ | 5993.2 | 0.76 | 3.1 | 6016.5 | 1.10 | 6031.5 | 1.16 |
| Ox catalyst | 5993.5 | 0.84 | 2.0 | Not resolved | | 6034.0 | 1.23 |

Data are referred to the dotted line spectra reported in Fig. 2. In the $CrO_3$ model compound a shoulder before the first edge feature is observed around 6009 eV having an intensity of 0.88.

Table 2
XANES features of the $Cr/SiO_2$ Phillips catalyst after reduction in CO at 623 K

| Pre-edge | | | | Edge | | | |
|---|---|---|---|---|---|---|---|
| Feature 1 (sh) | | Feature 2 | | Feature 3 (sh) | | White line | |
| Position (eV) | Intensity (norm. abs.) | Position (eV) | Intensity (norm. abs.) | Position (eV) | Intensity (norm. abs.) | Position (eV) | Intensity (norm. abs.) |
| 5988.3 | 0.05 | 5990.4 | 0.11 | 5995.9 | 0.47 | 6008.2 | 1.32 |

Data are referred to the black line spectrum reported in Fig. 2. After the white line an almost continuous absorption up to 6200 eV exists (sh, shoulder).

Table 3
XANES features of $\alpha$-$Cr_2O_3$ model compound

| Pre-edge | | | | Edge | | | | | |
|---|---|---|---|---|---|---|---|---|---|
| Feature 1 | | Feature 2 | | Feature 1 (sh) | | Feature 2 | | Feature 3 | |
| Position (eV) | Intensity (norm. abs.) | Position (eV) | Intensity (norm. abs.) | Position (eV) | Intensity (norm. abs.) | Position (eV) | Intensity (norm. abs.) | Position (eV) | Intensity (norm. abs.) |
| 5990.5 | 0.06 | 5993.6 | 0.12 | 6001.4 | 0.66 | 6007.3 | 1.42 | 6011.3 | 1.54 |

Data are referred to the gray line spectrum reported in Fig. 2. After the edge feature 3, a shoulder around 6016 eV (absorption = 1.21) and a defined component at 6024.5 eV (absorption = 1.19) are clearly visible (sh, shoulder).

cal of Cr(VI) with $T_d$-like symmetry, where the lack of an inversion center makes $A_1 \rightarrow E$ electronic transition Laporte allowed, as also happens with other $d^0$ systems like Ti(IV) [52,53]. A Cr(VI) with $T_d$-like symmetry is basically compatible with both chromate and dichromate structures. These main features were observed and discussed first by Weckhuysen et al. [10] and successively by other groups [34,35]. The high-energy resolution of the spectra reported here allows us to make some additional comparison with the XANES spectrum of the $CrO_3$ reference. The significant higher intensity of the $A_1 \rightarrow E$ pre-edge peak (0.84 vs. 0.76), together with a higher sharpness (the FWHM moves from 2.0 to 3.1 eV), suggests that Cr(VI) species grafted to silica have a more perfect $T_d$ symmetry than do those in $CrO_3$. A blue shift of 0.3 eV, which is at the limit of our actual energy resolution, has also been observed (see inset of Fig. 2 and Table 1). Of interest, as observed in the pre-edge component of both materials, is the presence of a low-energy tail, centered around 5991.3 eV. This minority component is relatively more intense in $CrO_3$. The model compound exhibits two well-defined edge features (at 6016.5 and 6031.5 eV) and a shoulder around 6009 eV, whereas only a broad absorption is observed for the oxidized catalyst.

The remarkable red shift of the edge of the CO-reduced catalyst (black line in Fig. 2), both with respect to the oxidized sample (about 6.5 eV) and with respect to the $\alpha$-$Cr_2O_3$ reference (about 2.0 eV), suggests that the CO-reducing process converts Cr(VI) into Cr species with an average oxidation state lower than +3, given by the simultaneous presence of Cr(II) (mainly) and Cr(III) species. This result agrees perfectly with the literature [3,5,7,12,18–27]. The pre-edge peak associated with tetrahedral Cr(VI) species totally disappears and is replaced by three distinct features at 5988.3 eV (vw), 5990.4 eV (w), and 5995.9 eV (s), the last being almost on the edge (Table 2). A similar shoulder has been observed for the $[Cr(OCOCH_3)_2 \cdot H_2O]_2$ Cr(II) model compound in planar square coordination [28] (reported only in the inset of Fig. 2, dashed line, for clarity). As a shoulder around 5995 eV is extrapolated from the CO-reduced $Cr/SiO_2$ catalyst reported in Fig. 7 of the work by Weckhuysen et al. [10], we can propose that the 5995.9 eV component is a fingerprint of Cr(II) species in an almost fourfold coordination state. A broad white line is observed with a maximum at 6008.2 eV (black line in Fig. 2). Details of the XANES features of $\alpha$-$Cr_2O_3$ model compound are summarized in Table 3. Because of the difference in both the oxidation and coordination states of chromium between the reduced

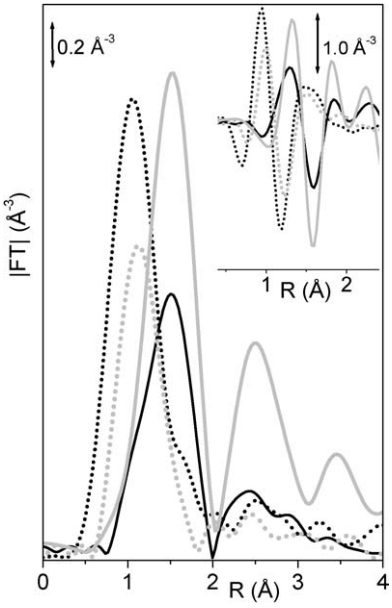


Fig. 3. Modulus of the $k^2$-weighted, phase-uncorrected, Fourier transform (|FT|, 2–11 $Å^{-1}$ range) of the EXAFS signal collected together with the XANES spectra reported in Fig. 2 (same symbols used). The inset reports, with the same symbols, the corresponding imaginary parts.

sample and the $\alpha$-$Cr_2O_3$ model, a comparison between the corresponding XANES features is not feasible.

From the XANES spectrum of the CO-reduced sample, two pieces of evidence confirm that a detectable amount of $Cr_2O_3$ clusters is present, because of the relatively high chromium loading (4 wt%): (i) the shoulder at 5995.9 eV, which is less pronounced than that observed for the $[Cr(OCOCH_3)_2 \cdot H_2O]_2$ model compound; (ii) the presence of an unstructured absorption in the 5990–5993-eV range (a region where pre-edge features of $\alpha$-$Cr_2O_3$ appear; see Table 3).

### 3.2.2. EXAFS data

Fig. 3 reports the $k^2$-weighted, non-phase-corrected, Fourier transform (FT) of the EXAFS functions of the $Cr/SiO_2$ catalyst and of the reference compounds collected together with the XANES spectra reported in Fig. 2 (the same symbols have been used). Three main peaks at 1.52, 2.49, and 3.46 Å (phase-uncorrected) are observed for the $\alpha$-$Cr_2O_3$ model compound (full gray curve), assigned to the first, second, and third shell contributions of a Cr(III) in an octahedral environment, respectively. Conversely, for $CrO_3$ (dotted gray curve) the main peak is observed at 1.12 Å (non-phase-corrected), coinciding with the Cr=O bond distance of a Cr(VI) in a tetrahedral environment. The absence of *d* electrons in Cr(VI) is responsible for much shorter Cr–O single bonds for $CrO_3$ if compared with those present in $\alpha$-$Cr_2O_3$. Furthermore, the intensity of the first shell signal in $CrO_3$ is much weaker if compared with that of $\alpha$-$Cr_2O_3$, and the higher shells contributions are almost completely absent. This suggests a greater disorder of the $CrO_4$ tetrahedron in $CrO_3$.

The oxidized catalyst (dotted black curve in Fig. 3) exhibits a dominant contribution centered at 1.06 Å (non-phase-corrected), which is clearly due to the short Cr=O double bonds, and, at greater distances (1.55 Å, non-phase-corrected), a shoulder due to longer Cr–O single bonds. On the basis of what was previously determined from UV–Vis, XRD, and XANES results, we can affirm that this signal is a complex one, as two families of species are present, resulting in three kind of contributions: Cr=O and Cr–O of isolated Cr(VI) and Cr–O of clustered Cr(III). This heterogeneity in distances implies, in *k*-space, the superposition of sinusoidal signals with a substantial difference in periodicity. Under such conditions the experimental $\chi(k)$ function is rapidly extinguished by out-of-phase signals and shows only noise for k values higher than 7 $Å^{-1}$. It is evident that such a short signal does not allow the extraction of any quantitative data in such a complex situation. It is worth noticing that this destructive interference mainly affects the Cr–O single bond signals, as the experimental |FT| is clearly dominated by the Cr=O contribution. This fact can be explained on the basis of three main factors: (i) the shorter distance of the oxygen atoms of the chromyl groups (the EXAFS signal scales with $1/R^2$); (ii) the stronger Cr=O bond, which is reflected by a smaller Debye–Waller factor; (iii) the amorphous nature of the support (and of the $Cr_2O_3$ nanoparticles), which induces a further increase, of static origin, in the measured Debye–Waller factor for the Cr–O bonds.

Weckhuysen et al. [10] measured and analyzed a similar sample reporting a Cr=O contribution at 1.53 Å ($N = 2.2$), a Cr–O contribution at 2.05 Å ($N = 2.1$), and a Cr–Cr contribution at 3.10 Å ($N = 0.5$) (actual distances). Based on the above discussion, we believe that the Cr–O and Cr–Cr contributions detected in Ref. [10] come from aggregated $Cr_2O_3$ particles. This interpretation is one of those reported by the authors of Ref. [10] and is supported by the more recent experimental results of Wang et al. [34]. These authors investigated much more Cr-diluted samples (in the 0.35–1.7 wt% range) supported on mesoporous MCM-41 in fluorescence mode. Under such diluted conditions, only a single peak is observed in the phase-uncorrected modulus of the FT (|FT|) of the oxidized samples at 1.23 Å, and no vestiges of the high-*R* component (shoulder in our sample and a well-defined component in the data of Ref. [10]) are present. This is further proof of the destructive interference occurring when both aggregated Cr(III) and dispersed Cr(II) species are present (vide supra and dotted curve in Fig. 3).

Upon reduction in CO at 623 K, the experimental $\chi(k)$ shows a significant signal up to 11 $Å^{-1}$ and its $k^2$-weighted, non-phase-corrected FT shows an almost symmetrical peak, centered at 1.51 Å, and the strong Cr=O signal has disappeared. After reduction, the Cr–O distances of the isolated species have undergone a significant elongation due to the large ionic radius of Cr(II) compared with that of Cr(VI) and are now much closer to those of the clustered species. The much higher *k* range at our disposal and the simplification of the system now allow the extraction of quantitative data, pro-

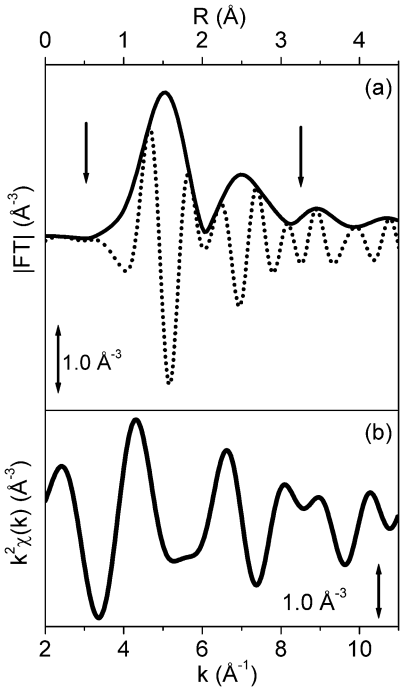


Fig. 4. (a) Modulus (full line) and imaginary part (dotted line) of the $k^2$-weighted, phase-uncorrected, Fourier transform of the EXAFS signal of $\alpha$-$Cr_2O_3$ model compound. The two arrows indicate the $R$-range used to extract the filtered first shell signals of $\alpha$-$Cr_2O_3$ reported in part (b).

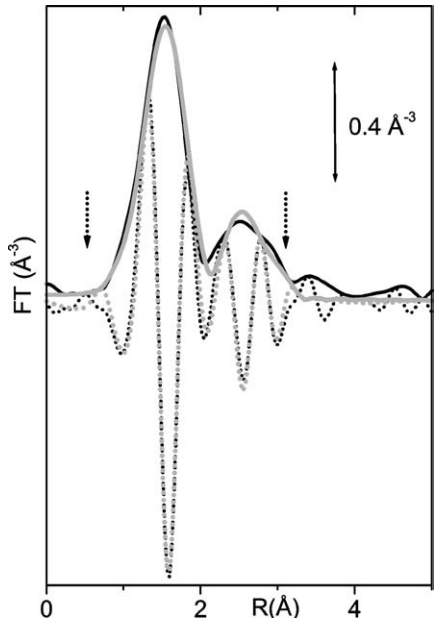


Fig. 5. Comparison between experimental (black) and model (gray) for the $k^2$-weighted FT of the EXAFS signal of the CO-reduced catalyst. Full and dotted lines refer to modulus and imaginary part, respectively. Dotted arrows indicate the fit range.

vided that the presence of aggregated $Cr_2O_3$ species is taken into account. The analysis has been conducted following the methodology discussed in Section 2.2, where the two phases present are isolated Cr(II) species grafted to the silica support and aggregated Cr(III) species, respectively. To reduce the number of fitting parameters we have imposed chemical constraints and thus assumed that the aggregated Cr(III) species have an $\alpha$-$Cr_2O_3$-like local structure. Under these assumptions, the two relationships discussed in Section 2.2 now become:

$$N_{\text{fit}}(\alpha\text{-}Cr_2O_3) = N(\alpha\text{-}Cr_2O_3)x,$$

$$N_{\text{fit}}(\text{Cr(II)}_{\text{isolated}}) = N(\text{Cr(II)}_{\text{isolated}})(1-x).$$

Briefly summarizing, the EXAFS quantitative analysis was conducted as follows: (i) Starting from the FT of the EXAFS signal of the $\alpha$-$Cr_2O_3$ model compound (Fig. 4a), the inverse FT has been performed in the 0.51–3.13-Å range (see vertical arrows in Fig. 4a). This results in the filtered $\chi(k)$ function reported in Fig. 4b, representing the sum of the contribution of all of the scattering due to atoms in the first, the second, and part of the third coordination shells around Cr(III) in $\alpha$-$Cr_2O_3$. Note that in this approach both single and multiple scattering paths are included. (ii) The signal thus obtained was then used for the extraction of "fictitious" phases and amplitudes that do not refer to a single Cr-scatterer contribution, but reflects the local environment of Cr atoms in the aggregated phase in an overall way. (iii) The aggregated Cr(III) species have been fitted by using the so obtained phase and amplitudes, leaving $N$, DW, and $\Delta E$ as free parameters. In this case, the $N_{\text{fit}}(\alpha\text{-}Cr_2O_3)$ directly resulted in the fraction $x$ of aggregated species present in the catalyst, according to the relationship reported above. The DW factors have been allowed to change, in contrast to the study of Prestipino et al. [47] (where the size of the crystals of the aggregated phase was huge), to take into account that a significant fraction of the $Cr_2O_3$ particles have a very small size, as determined by a comparison of UV–Vis and XRD data (Fig. 1b). This is a crude way to consider the distributions of bond lengths due to particle heterogeneity with the use of a unique fitting parameter. (iv) The isolated Cr(II) species have been fitted with a single Cr–O contribution, leaving $N$, $R$, DW, and $\Delta E$ as free parameters; such values have thus to be considered on an average ground. Because of the amorphous nature of the support, isolated Cr(II) species are not supposed to contribute to the EXAFS signal at higher $R$ values, so that, in the 2.15–3.13-Å range, only clustered species contribute to the experimental signal. This assumption is supported by the fact that no higher shell signal has been observed by Wang et al. [34] for samples containing only isolated chromium species.

The fraction of $\alpha$-$Cr_2O_3$-like particles was estimated to be $x = 0.38 \pm 0.04$, and the DW increased from 0.0050 to $0.0065 \pm 0.0005$ Å$^2$, supporting the presence of small clusters. For the isolated Cr(II) species, we obtained a Cr–O contribution at $1.96 \pm 0.01$ Å, with a coordination number of $3.6 \pm 0.3$ and a DW of $0.0075 \pm 0.0006$ Å$^2$. The quality of the fit can be appreciated in Fig. 5, where we report both imaginary part and modulus of the experimental $k^2$-weighted FT superimposed on the model (sum of isolated and clustered species).

### 3.3. Catalyst after in situ polymerization

#### 3.3.1. XANES data

When the CO-reduced model catalyst is brought into contact with $C_2H_4$ at room temperature, the polymerization process starts almost immediately [4,5,15,25,36,37]. This fact has been clearly indicated in many time-resolved, in situ IR experiments [5,25,36,37], where the intensity of the stretching bands of the $CH_2$ species has been observed to increase as a function of time, with a constant increase after the first 50–100 s [36]. During this first time polymers are well observed, but their growth rate is significantly lower, because of the formation of polymer precursor species [5]. The response of the IR spectroscopy is intrinsically related to the working sites only, as the polymerization occurs only there. We have repeated in our XAFS cell [38] the same polymerization experiment investigated many times with IR spectroscopy. The XANES spectrum of the CO-reduced model catalyst after polymerization (dashed curve in Fig. 6) exhibits a slight increase in the intensity of the white line with respect to the spectrum collected prior to polymerization (full line spectrum in Fig. 6), which reflects a modest increase in the average coordination of Cr(II) ions. In the pre-edge region (see inset of Fig. 6) we observe a decrease in the fingerprint of Cr(II) species at 5995.9 eV.

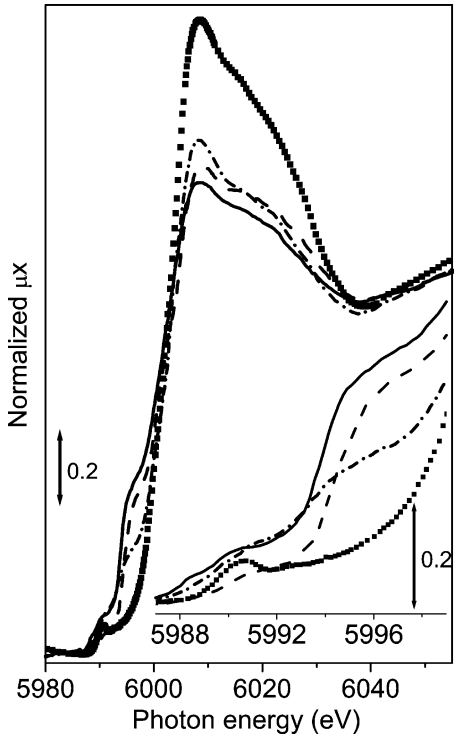


Fig. 6. High resolution XANES spectra of the catalyst after in situ polymerization. The dashed line and the dash-dotted line spectra refer to the CO reduced sample, subsequently contacted with $C_2H_4$ at RT and at 373 K, respectively. The scattered square line refers to the $Cr/SiO_2$ catalyst directly reduced in $C_2H_4$ at 523 K for 1 h (ethylene-reduced catalyst). As an example of unengaged Cr(II) species, the spectrum collected on the CO reduced catalyst (prior contact with ethylene) is also reported (full line). The inset reports a magnification of the pre-edge features.

These results suggest that the number of Cr(II) sites involved in the polymerization reaction at room temperature (and low ethylene pressure) is very low, so that the XANES spectrum after polymerization reflects the majority of inactive chromium sites and only slight modification is present with respect to the sample prior to polymerization. Of course, we have to remember that we are in the presence of about 40% of $Cr_2O_3$ clusters, so that the XANES spectrum is better described as a mixture of Cr(III) species, unreacted Cr(II) species, and chromium sites at a higher oxidation state (presumably IV) due to the presence of polymer chains. As far as the last species are concerned, most of the hypothesized reaction mechanisms describe the living chromium site as a Cr(IV) site coordinated with two support oxygen atoms and two carbon atoms of the growing polymer chain [5,54–56].

As discussed in the Introduction, the industrial polymerization procedure consists of the admission of ethylene directly on the oxidized catalyst in the 373–423 K interval. By adopting a similar procedure (here $C_2H_4$ has been dosed at 523 K, squared line in Fig. 6), we observe the depletion of the pre-edge peak characteristic of Cr(VI) in a $T_d$-like geometry and a shift of the edge toward lower energy values with respect to the oxidized starting point (dotted black line in Fig. 2). This confirms that Cr(VI) is reduced by ethylene during the polymerization reaction. Unfortunately, as discussed before, the situation is complicated by the presence of 40% of clustered Cr(III) species, so that it is difficult to estimate the average oxidation state of chromium in the ethylene-reduced sample. However, from a comparison of the spectrum of the ethylene-reduced catalyst (squared line in Fig. 6) with that of the model system after polymerization (dashed line in Fig. 6), the following observations can be made: (i) the intensity of the white line grows remarkably, reflecting a much higher increase in the average chromium coordination; (ii) the Cr(II) fingerprint feature at 5996 eV is totally absent, suggesting that almost all isolated chromium species have been involved in the polymerization reaction. Some considerations concerning the technique must be discussed here. The fact that the Cr(II) fingerprint feature at 5996 eV is totally absent in the ethylene-reduced catalyst reflects that the polymerization perturbed almost all of the isolated chromium sites, but this does not mean that all sites are active in catalysis. A large heterogeneity is expected among the isolated Cr species at this stage [5], including active Cr sites carrying the polymer chains, Cr sites just perturbed by a polymer generated elsewhere, Cr sites still in interaction with reduction products, or, eventually, Cr sites carrying some “deactivating precursors” (such as Cr-cyclopentane structures, which have been found to be inactive with respect to polymerization [57]).

By bringing the model catalyst into contact with ethylene at 373 K, we obtained a XANES spectrum (dash-dotted line in Fig. 6) with both a white line and a Cr(II) finger-

print shoulder, which are intermediate between the two cases discussed above. Thus, we conclude that the number of chromium sites involved in the polymerization reaction increases in the order model catalyst at RT < model catalyst at 373 K < ethylene-reduced catalyst at 523 K. Note that in the case of the reduced catalyst, where no reduction products are supposed to be present, the decrease in the Cr(II) fingerprint at 5996 eV may be used to evaluate an upper limit of the number of Cr(II) sites active in the polymerization. By comparing the integrated area of the 5996 eV band in the case of the model catalyst after polymerization at RT with that of the model catalyst before polymerization, we estimated that a fraction of about 25% of the original Cr(II) sites has been involved in the polymerization. Analogously, when the polymerization is performed on the model catalyst at 373 K, about 55% of the initial Cr(II) sites are involved in the polymerization. Even if these values do not correspond directly with the fraction of really active sites, they suggest the order of magnitude of the active sites, which is probably near 10% of the Cr(II) sites. These numbers are in quantitative agreement with the number of engaged Cr sites as evaluated by IR spectroscopy (35 vs. 25% and 52 vs. 55%). Engaged Cr sites have been evaluated from IR experiments by quantification of the intensity of the CO triplet, in the 2191–2178 $cm^{-1}$ range, before and after polymerization (unpublished results).

### 3.3.2. EXAFS data

The picture emerging from XANES is qualitatively confirmed by EXAFS (Fig. 7), where the $k^2$-weighted, non-phase-corrected FT of the EXAFS signals (2–11 $Å^{-1}$ range) collected on the $Cr/SiO_2$ catalyst after polymerization is reported. The intensity of the peak in the 0.7–2.0-Å interval increases in the order reduced model catalyst (full line) < model catalyst polymerized at RT (dashed line) < model catalyst polymerized at 373 K (not reported for clarity) < ethylene-reduced catalyst (scattered squares). EXAFS is unable to discriminate between Cr–O and Cr–C first shell contributions. However, as we do not expect a change in the Cr-to-support interactions, the increase in the peak at 0.7–2.0 Å is attributed to an increase in the average number of C atoms entering the first coordination shell of isolated Cr species upon polymerization.

The heterogeneity of Cr species under polymerization conditions prevented any attempt to obtain quantitative data from the corresponding EXAFS spectra, and the discussion has to be concluded on the qualitative ground reported above. As for the ethylene-reduced catalyst, we can just add that the inability to reproduce the second shell contribution with the $\alpha$-$Cr_2O_3$ signal, as done for the model catalyst (Fig. 5), suggests that a significant fraction of the experimental contribution in the 2.0–3.2-Å range comes from the polymerization products.

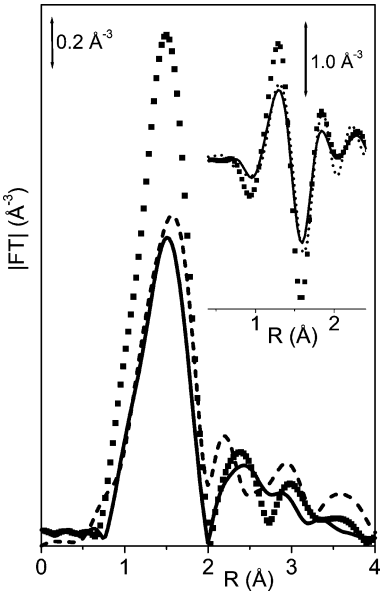


Fig. 7. Modulus of the $k^2$-weighted, phase-uncorrected, Fourier transform (2–11 $Å^{-1}$ range) of the EXAFS signal collected together with the XANES spectra reported in Fig. 6 (same symbols used). The inset reports, with the same symbols, the corresponding imaginary parts.

### 3.4. Preliminary ReflEXAFS data on the $CrO_x/SiO_2/Si(100)$ model system

A preliminary study in the direction of investigating a less heterogeneous system has been conducted on a $CrO_x/SiO_2/Si(100)$ model catalyst (nominal Cr loading of 4 Cr atoms/$nm^2$) prepared ex situ, characterized by an almost molecular dispersion of Cr species [6,16,17]. Because the Cr species are supported on a flat silica surface, the ReflEXAFS geometry has been adopted [46,58]. The XANES spectrum of the $CrO_x/SiO_2/Si(100)$ model catalyst after the ex situ thermal activation at 723 K in dry oxy-

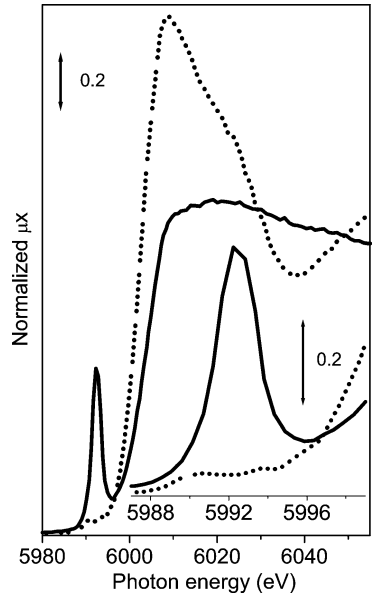


Fig. 8. XANES spectra of $CrO_x/SiO_2/Si(100)$ model catalyst after thermal activation (full line) and after polymerization (dotted line), collected ex situ in ReflEXAFS mode.

gen (full line in Fig. 8) shows the pre-edge peak peculiar to Cr(VI) in a $T_d$-like geometry. After this thermal treatment about 2 Cr/nm$^2$ are present exclusively as surface monochromates that are anchored to the silica surface via two ester bonds. The superfluous chromium desorbs from the surface, preventing the formation of $Cr_2O_3$ clusters. The Cr(VI) pre-edge feature is less intense and less resolved than that observed on the $Cr/SiO_2$ catalyst (dotted black line in Fig. 2). No features can be distinguished at the edge region, possibly because of a lack of photon counts. This sample was exposed to the air during transfer to the ReflEXAFS chamber, which inevitably results in poisoning with water, oxygen, and airborne carbon contaminants. This in turn has undeniably degraded the sample to some extent, by hydrolysis of the Cr–O–Si ester linkages and by partial reduction of the surface chromate (VI) species, which are exclusively present on the pristine model-catalyst surface after calcinations [6,17].

The second ReflEXAFS spectrum presented in Fig. 8 (dotted line) shows model catalyst after a 1-h polymerization run at 433 K at 1 bar of ethylene pressure following a thermal activation at 723 K. In this sample the catalyst surface is protected from the ambient by a 600-nm-thick layer of polyethylene that has formed during the polymerization run. The XANES obtained presents features very similar to those discussed above for the ethylene-reduced $Cr/SiO_2$ system (scattered squares in Fig. 6), in both the pre-edge and edge regions. The greater intensity of the white line (1.77 vs. 1.66) can be explained by the fact that, thanks to the almost atomic dispersion of Cr sites, we do not have here the fraction of aggregated Cr species for which the XANES spectrum is characterized by a lower white line intensity (see Table 3). The fact that the $CrO_x/SiO_2/Si(100)$ model catalyst presents the same behavior during polymerization and gives rise to the same XANES features as the standard $Cr/SiO_2$ catalyst is worth noticing, as it is commonly known that small modifications in the catalyst preparation, treatment procedure, polymerization conditions, etc. have a great influence on catalyst activity [5].

## 4. Conclusions

In this work we report an improved version of the transmission X-ray absorption experiments performed so far on the $Cr/SiO_2$ catalysts [10,35]. The work presents several novel elements, from a catalytic as well as a technical point of view, which are resumed in the following:

(i) On the catalytic side, we report the first quantitative estimation of the fraction of clustered $Cr_2O_3$ particles, unavoidably present under the Cr loading needed to allow transmission measurements. Even if the presence of $Cr_2O_3$ particles in samples with such a high Cr loading was perfectly known in the literature, this quantitative result is particularly important for preventing a misleading interpretation of past and future XAS results for analogous $Cr/SiO_2$ systems.

(ii) We report the first XANES/EXAFS in situ study on the catalyst after polymerization, investigating the effect of different polymerization procedures (model vs. ethylene-reduced). We demonstrate that it is possible to monitor the fraction of Cr sites involved in the polymerization reaction and to estimate an upper limit of the active Cr(II) sites by means of a XANES technique, by following the erosion of the Cr(II) fingerprint at 5996 eV and the increase in the white line intensity. Fractions of about 25 and 55% of the original Cr(II) sites have been estimated to be involved when ethylene polymerization is performed on the model catalyst at room temperature and at 373 K, respectively.

(iii) On the technical side, the use of a third-generation synchrotron radiation source has allowed us to improve the both the energy resolution and the signal-to-noise ratio of the XANES data, compared with the literature on XAS for Phillips catalyst or related systems [10,34,35].

The main limit of this study consists of the presence of a fraction of clustered $Cr_2O_3$ particles that prevents any structural EXAFS data analysis of the samples after polymerization and that influences the reported XANES features at each stage of the study. We demonstrated that a two-phase analysis of the EXAFS spectra is possible, but only on systems with a limited degree of complexity. It is therefore evident that the next generation of XANES/EXAFS experiments on this catalyst must be performed in fluorescence mode on a more diluted sample to avoid the formation of $Cr_2O_3$ particles. Preliminary results in this direction are reported in Section 3.4.

## Acknowledgments

We are indebted to A. Agostino for XRD measurements and to the whole staff of the GILDA BM8 beamline at the ESRF (in particular F. D'Acapito, F. La Manna, and F. D'Anca) for their important support during XAS experiments. The economic support of the INFM PURS project is acknowledged.

## References

[1] J.P. Hogan, R.L. Banks, 1958.
[2] K.H. Theopold, Chemtech 27 (1997) 26.
[3] B.M. Weckhuysen, R.A. Schoonheydt, Catal. Today 51 (1999) 215.
[4] M.P. McDaniel, Adv. Catal. 33 (1985) 47.
[5] E. Groppo, C. Lamberti, S. Bordiga, G. Spoto, A. Zecchina, Chem. Rev. 2004, in press.
[6] E.M.E. van Kimmenade, A.E.T. Kuiper, Y. Tamminga, P.C. Thune, J.W. Niemantsverdriet, J. Catal. 223 (2004) 134.
[7] A. Zecchina, E. Garrone, G. Ghiotti, C. Morterra, E. Borello, J. Phys. Chem. 79 (1975) 966.
[8] M. Nishimura, J.M. Thomas, Catal. Lett. (1993) 149.

[9] M.A. Vuurman, I.E. Wachs, D.J. Stufkens, A. Oskam, J. Mol. Catal. 80 (1993) 209.
[10] B.M. Weckhuysen, R.A. Schoonheydt, J.M. Jehng, I.E. Wachs, S.J. Cho, R. Ryoo, S. Kijlstra, E. Poels, J. Chem. Soc. Faraday Trans. 91 (1995) 3245.
[11] C. Groeneveld, P.P.M.M. Wittgen, A.M. van Kersbergen, P.L.M. Hestrom, C.E. Nuijten, G.C.A. Schuit, J. Catal. 59 (1979) 153.
[12] B. Rebenstorf, R. Larsson, J. Mol. Catal. 11 (1981) 247.
[13] B.M. Weckhuysen, I.E. Wachs, R.A. Shoonheydt, Chem. Rev. 96 (1996) 3327.
[14] A. Zecchina, E. Garrone, G. Ghiotti, S. Coluccia, J. Phys. Chem. 79 (1975) 972.
[15] R. Merryfield, M.P. McDaniel, G. Parks, J. Catal. 77 (1982) 348.
[16] P.C. Thune, C.P.J. Verhagen, M.J.G. van den Boer, J.W. Niemantsverdriet, J. Phys. Chem. B 101 (1997) 8559.
[17] P.C. Thune, R. Linke, W.J.H. van Gennip, A.M. de Jong, J.W. Niemantsverdriet, J. Phys. Chem. B 105 (2001) 3073.
[18] B. Fubini, G. Ghiotti, L. Stradella, E. Garrone, C. Morterra, J. Catal. 66 (1980) 200.
[19] B.M. Weckhuysen, A.A. Verberckmoes, A.R. DeBaets, R.A. Schoonheydt, J. Catal. 166 (1997) 160.
[20] B.M. Weckhuysen, L.M. Deridder, R.A. Schoonheydt, J. Phys. Chem. 97 (1993) 4756.
[21] P. Zielinski, I.G.D. Lana, J. Catal. 137 (1992) 368.
[22] C.S. Kim, S.I. Woo, J. Mol. Catal. 73 (1992) 249.
[23] G. Spoto, S. Bordiga, E. Garrone, G. Ghiotti, A. Zecchina, G. Petrini, G. Leofanti, J. Mol. Catal. 74 (1992) 175.
[24] G. Ghiotti, E. Garrone, G. Della Gatta, B. Fubini, E. Giamello, J. Catal. 80 (1983) 249.
[25] A. Zecchina, D. Scarano, S. Bordiga, G. Spoto, C. Lamberti, Adv. Catal. 46 (2001) 265.
[26] G. Ghiotti, E. Garrone, A. Zecchina, J. Mol. Catal. 65 (1991) 73.
[27] A. Zecchina, G. Spoto, G. Ghiotti, E. Garrone, J. Mol. Catal. 86 (1994) 423.
[28] A. Pantelouris, H. Modrovw, M. Pantelouris, J. Hormes, D. Reinen, Chem. Phys. 300 (2004) 13.
[29] C. Jousseaume, F. Ribot, A. Kahn-Harari, D. Vivien, F. Villain, Nucl. Instrum. Meth. B 200 (2003) 425.
[30] C. Jousseaume, D. Vivien, A. Kahn-Harari, J. Derouet, F. Ribot, F. Villain, J. Appl. Phys. 93 (2003) 6006.
[31] I. Arcon, B. Mirtic, A. Kodre, J. Am. Chem. Soc. 81 (1998) 222.
[32] J. Wong, F.W. Lytle, R.P. Messmer, D.H. Maylotte, Phys. Rev. B 30 (1984) 5595.
[33] L. Garcia, M. Benfatto, C.R. Natoli, A. Bianconi, I. Davoli, A. Marcelli, Solid. State Commun. 58 (1986) 595.
[34] Y. Wang, Y. Ohishi, T. Shishido, Q.H. Zhang, W. Yang, Q. Guo, H.L. Wan, K. Takehira, J. Catal. 220 (2003) 347.
[35] C. Pak, G.L. Haller, Micropor. Mesopor. Mater. 48 (2001) 165.
[36] G. Ghiotti, E. Garrone, A. Zecchina, J. Mol. Catal. 46 (1988) 61.
[37] S. Bordiga, S. Bertarione, A. Damin, C. Prestipino, G. Spoto, C. Lamberti, A. Zecchina, J. Mol. Catal. A 204 (2003) 527.
[38] C. Lamberti, C. Prestipino, S. Bordiga, G. Berlier, G. Spoto, A. Zecchina, A. Laloni, F. La Manna, F. D'Anca, R. Felici, F. D'Acapito, P. Roy, Nucl. Instrum. Meth. B 200 (2003) 196.
[39] C. Lamberti, G. Spoto, D. Scarano, C. Paze, M. Salvalaggio, S. Bordiga, A. Zecchina, G. Turnes Palomino, F. D'Acapito, Chem. Phys. Lett. 269 (1997) 500.
[40] G. Turnes Palomino, P. Fisicaro, S. Bordiga, A. Zecchina, E. Giamello, C. Lamberti, J. Phys. Chem. B 104 (2000) 4064.
[41] G. Berlier, G. Spoto, P. Fisicaro, S. Bordiga, A. Zecchina, E. Giamello, C. Lamberti, Microchem. J. 71 (2002) 101.
[42] G. Berlier, G. Spoto, S. Bordiga, G. Ricchiardi, P. Fisicaro, A. Zecchina, I. Rossetti, E. Selli, L. Forni, E. Giamello, C. Lamberti, J. Catal. 208 (2002) 64.
[43] C. Lamberti, S. Bordiga, F. Bonino, C. Prestipino, G. Berlier, L. Capello, F. D'Acapito, F.X. Llabres i Xamena, A. Zecchina, Phys. Chem. Chem. Phys. 5 (2003) 4502.
[44] K.V. Klementev, J. Phys. D, Appl. Phys. 34 (2001) 209.
[45] K.V. Klementev, J. Phys. D, Appl. Phys. 34 (2001) 2241.
[46] F. D'Acapito, I. Davoli, P. Ghigna, S. Mobilio, J. Synchrotron Rad. 10 (2003) 260.
[47] C. Prestipino, S. Bordiga, C. Lamberti, S. Vidotto, M. Garilli, B. Cremaschi, A. Marsella, G. Leofanti, P. Fisicaro, G. Spoto, A. Zecchina, J. Phys. Chem. B 107 (2003) 5022.
[48] G. Turnes Palomino, S. Bordiga, A. Zecchina, G.L. Marra, C. Lamberti, J. Phys. Chem. B 104 (2000) 8641.
[49] C. Lamberti, C. Prestipino, S. Bordiga, A.N. Fitch, G.L. Marra, Nuclear Instrum. Meth. B 200 (2003) 155.
[50] M. Cieslak-Golonka, Coordin. Chem. Rev. 109 (1991) 223.
[51] D. Scarano, G. Spoto, S. Bordiga, L. Carnelli, G. Ricchiardi, A. Zecchina, Langmuir 10 (1994) 3094.
[52] G. Ricchiardi, A. Damin, S. Bordiga, C. Lamberti, G. Spano, F. Rivetti, A. Zecchina, J. Am. Chem. Soc. 123 (2001) 11409.
[53] S. Bordiga, S. Coluccia, C. Lamberti, L. Marchese, A. Zecchina, F. Boscherini, F. Buffa, F. Genoni, G. Leofanti, G. Petrini, G. Vlaic, J. Phys. Chem. 98 (1994) 4125.
[54] S.L. Scott, J. Amor Nait Ajjou, Chem. Eng. Sci. 56 (2001) 4155.
[55] J. Amor Nait Ajjou, G.L. Rice, S.L. Scott, J. Am. Chem. Soc. 120 (1998) 13436.
[56] B. Liu, H. Nakatani, M. Terano, J. Mol. Catal. A 184 (2002) 387.
[57] O. Espelid, K.J. Borve, J. Catal. 205 (2002) 366.
[58] C. Lamberti, Surf. Sci. Rep. 53 (2004) 1.